Theor Chem Acc (2009) 124:235–250
DOI 10.1007/s00214-009-0604-2

REGULAR ARTICLE

A theoretical study about the structural, electronic and spectroscopic properties of the ground and singlet excited states of curcuminoidic core

Enrico Benassi · Ferdinando Spagnolo

Received: 21 January 2009 / Accepted: 3 July 2009 / Published online: 18 July 2009

Abstract Curcumin, a well-known Indian spice, holds a variety of properties in many different fields from medicinal chemistry to dye industry. The peculiar electronic structure makes curcumin a valuable metal chelator. The principal aim of this work is a computational study of the structural and electronic properties of the ground and the first singlet excited states of the curcuminoidic core. Concerning the ground state, tautomeric equilibrium, vibrational and thermochemical analysis and electronic absorption spectra (with ab initio and semi-empirical methodologies) have been studied. A full geometry optimization of the first singlet excited states was obtained, with different computational methodologies. Solvent effects are also implicitly considered. An accurate comparison of the results is presented. Interesting aspects emerge, which suggest successive investigation about the nature of the excited states. The obtained results may be of large applicative interest. If curcuminoids are considered as potential ligands for complexes formation with metallic ions of pharmaceutical, medical–physical and technological interest, exciting the system with photons of appropriate frequencies, a photomodulated release of the metallic ion in the environment might be guessed, because of an important photoinduced geometrical modification.

E. Benassi (✉) · F. Spagnolo
Dipartimento di Chimica,
Università degli Studi di Modena e Reggio Emilia,
Modena, Italy
e-mail: enrico.benassi@libero.it

E. Benassi
School of Chemistry and Biochemistry,
Georgia Institute of Technology, Atlanta, GA, USA

Keywords Curcuminoid · 1,7-Diphenyl-5-hydroxy-1,4,6-heptatrien-3-one · 1,7-Diphenyl-1,6-heptadiene-3,5-dione · Electronic excited states optimization · Configuration interaction (CI-S) · Time-dependent SCF (TD-SCF) · Complete active space multiconfiguration SCF (CAS-SCF) · Density functional theory (DFT) · CS INDO CI

1 Introduction

Curcumin (Scheme 1a) is a widely diffused organic colouring spice and ingredient, being obtained from the dried rhizomes of *Curcuma longa* L. During the last few decades, this molecule and its derivatives have been utilized in biological and pharmaceutical fields, because of its remarkable anti-tumour, anti-oxidant, anti-arthritic, anti-amyloid, anti-ischaemic and anti-inflammatory properties [1, 2].

The peculiar electronic structure makes curcumin a valuable metal chelator. The β-keto-enolic function is capable of forming a coordinative bond with metals such as iron, copper and gallium. The metal chelating feature is being taken into the interest of pharmaceutical researchers to develop metal-complexes to be employed as pharmaceuticals for a variety of pathologies such as Alzheimer disease (complexing with copper), anti-cancer therapy (complexing with gallium), and iron deficiency pathologies (complexing with iron). The electronic properties of curcumin, however, may be useful even for developing new drugs for metal overload treatments such as hemochromatosis, when used in the ligand form [3].

In particular, when curcumin is chelated with metal ions such as Cu(II) [4] holds an interesting ROS scavenging ability [5], this property might be a valuable enhancer of

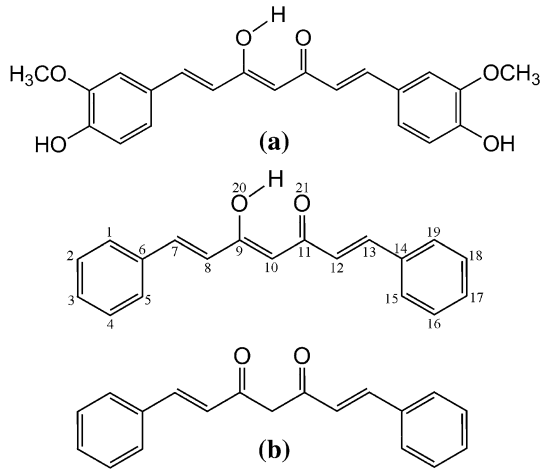

Scheme 1 **a** Curcumin in its most stable keto-enolic conformer. **b** Simplified Curcuminoidic structures: 1,7-diphenyl-5-hydroxy-1,4,6-hepta-trien-3-one (DPHHTO; *top*) and 1,7-diphenyl-1,6-heptadiene-3,5-dione (DPHDDO; *bottom*)

the proved biological activity of curcumin [6]. It is assessed that curcumin is a valuable iron chelating agent [7] and, since tumour cells growth is enhanced with high iron concentration, iron chelation can be valuable for anti-tumoural therapies as happens with other iron chelators [8].

Our recent study [9] has emphasized the importance of the poly-excited configurations and the effects caused by the interaction of curcumin and solvent in the description of the UV–Vis spectra and of some singlet excited states. In this work, we will explore with major detail the geometries of the first singlet excited electronic states of the curcuminoidic core and the influence the solvent holds in such contest. For these aims, the geometries optimizations were dealt following three different procedures. A detailed exploration of the geometrical characteristics of the excited states may be of large applicative interest, in particular concerning curcuminoids usefulness in coordination complexes formation. As emerges from the discussion of the theoretical results, this aspect, actually, holds important implications for potential pharmacological and medical applications.

Owing to that emerged in the Ref. [9] about the tiny differences of results obtained for the four rotamers of curcumin, and in order to simplify the problem treatment, as hinted above, it was decided not to refer exactly to curcumin *tout court*, but to a curcuminoidic more simple structure, the 1,7-diphenyl-5-hydroxy-1,4,6-heptatrien-3-one (DPHHTO; Scheme 1b, top), which does not present hydroxylic and methoxylic groups on the terminal phenyls, therefore it may be studied as a unique rotamer. For reasons of thoroughness, initially its diketo-isomer, the 1,7-diphenyl-1,6-heptadiene-3,5-dione (DPHDDO; Scheme 1b, bottom), was not neglected, even if ignoring its presence might be legitimated, on the basis of previous results on curcumin [10].

2 Computational details

A full geometry optimization of the electronic ground state at density functional theory (DFT) level using 6-311g(*p*,*d*), 6-311++g(3*df*,3*pd*), lanl2dz, dgtzvp and aug-cc-pv6z basis sets and considering B3-LYP functional was employed in order to obtained the forms of DPHHTO and DPHDDO in vacuum. Moreover, because DFT provides good geometries, as well known, starting with the respective DFT optimized geometries, also full fourth order Møller–Plesset perturbation theory (with single, double, triple and quadruple substitutions) single point calculations MP4(sdtq) and coupled cluster [using both single and double substitutions, including triple excitations non-iteratively for both the complete MP4 and to form CCSD(T)] single point calculations CCSD(t,e4t) with the previously cited basis sets were run, in order to obtain the total electronic energies for the two tautomers, and the relative differences. Since the tautomeric equilibrium seemed reasonably well described even employing the DFT B3-LYP/6-311g(*p*,*d*) approach, and in order to contain the computational costs, this was chosen as theory level for the successive calculations. The DFT B3-LYP/6-311g(*p*,*d*) optimized geometries were submitted to vibrations calculation in order to investigate whether the convergence points were "genuine" energy minima. This study was conducted both in vacuum and in solvent. The solvents effects were evaluated adopting the self-consistent reaction field (SCRF) method with polarized continuum model (PCM) [11–13]. The considered solvents were dimethyl sulfoxide (DMSO) and methanol.

On the basis of the previous results, the total electronic energies (E), the total electronic energies corrected with zero point vibrational energies ($E + \hbar\omega/2$), Gibbs free energies (G) and enthalpies (H) were calculated at DFT B3-LYP/6-311g(*p*,*d*) ab initio level of theory for the electronic ground state. Using the obtained thermodynamical parameters, the relative differences and Boltzmann's factors for the relative abundances in vacuum and in solvent at room temperature were calculated and analysed. Environmental conditions were set $T =$ 298.150 K and $p = 1.00$ atm.

For the most stable isomer in vacuum, the two dihedral angles of the phenyls were varied from the equilibrium value to $\pi/2$ radiants, with step of $\pi/6$ radiants, in order to track the energy profile. The energy values were obtained with single point B3LYP/6-311g(*p*,*d*) calculations on the constrained geometries. The energy differences with respect to the final optimized geometry and Boltzmann's factors at $T = 298.150$ K were calculated. Gaussian 03 computational package [14] was used for all the above mentioned calculations.

Successively, the electronic absorption spectra were calculated for the most stable isomer at configuration interaction (CI-S) DFT level [15], at the time-dependent DFT (TD-DFT) level and, as comparison, with the CS INDO CI method [16], which treats valence–shell states only and provided the best results for curcumin [9]. About CS INDO CI computational details, a similar approach to Ref. [9] was followed. The calculations of the singlet excited electronic states and, in consequence, the $S_0 \rightarrow S_n$ ($n = 1, 2,\ldots, 8$) absorption spectra, on the DPHHTO isomer were performed. The optimized geometry of the ground electronic state, as obtained from DFT calculations, was used in the CS INDO CI calculations. These calculations were performed considering Slater orbitals, Ohno-Klopman and Mataga-Nishimoto parameterizations for integrals and, when required, Miertus-Kysel model [17–20] for the solvent effect. The configuration interactions were carried out both in the singly-excited (S-CI) and in involving multiple excitations (SDT-CI) schemes. A MOs active space in the CI calculations included 30 occupied MOs and 30 virtual MOs. Some crucial full MOs calculations were also performed. For SDT-CI calculations about 2000 configurations were considered. Then the UV-Vis spectra were compared with the DFT ones. Such preliminary investigation was particularly important in the case of CAS-SCF optimization, because it allowed to understand the composition of the excited states and to select the active space correctly and differently for each state.

Then three different approaches were followed in order to obtain a full geometry optimization of the first eight electronic singlet excited states: the CI-S, the TD-SCF and the Complete Active Space Multiconfiguration SCF (CAS-SCF). Gaussian 03 computational package [14] was used for all these calculations. Each state was optimized starting from the DFT optimized geometry for the ground state, and choosing a different opportune active space, on the basis of the above said study of the electronic spectrum of DPHHTO. The number of electrons (N) and the number of MOs (M) in the active space were respectively $N = 6$ and $M = 6$ (occupied MOs: 71, 72, 73 $\equiv H$; unoccupied MOs: 74 $\equiv L$, 75, 76) for S_1, $N = 8$ and $M = 8$ (occupied MOs: 69, 71, 72, 73 $\equiv H$; unoccupied MOs: 74 $\equiv L$, 75, 76, 77) for S_2, $N = 10$ and $M = 10$ (occupied MOs: 68, 69, 71, 72, 73 $\equiv H$; unoccupied MOs: 74 $\equiv L$, 75, 76, 77, 78) for S_3, $N = 10$ and $M = 10$ (same active space of S_3) for S_4, $N = 8$ and $M = 8$ (same active space of S_2) for S_5, $N = 8$ and $M = 8$ (same active space of S_2) for S_6, $N = 10$ and $M = 10$ (same active space of S_3) for S_7, and $N = 8$ and $M = 8$ (same active space of S_2) for S_8. The MOs number is referred to the numeration as well as obtained by the previous DFT B3-LYP/6-311 g(p,d) calculations. The optimized geometries were submitted to vibrations calculation.

3 Results and discussion

In the following section, the computational results on DPHHTO and DPHDDO are presented and discussed, starting with the isomeric equilibrium and the analysis of the thermodynamics, structural and electronic properties of the ground state in vacuum, in comparisons with experimental literature data. Then the calculated absorption spectra and the wave-functions for the first singlet excited states are exposed. Therefore, the analysis of energetic, structural and electronic properties of the electronic excited states follows. Finally, the solvent effects are shown.

3.1 Isomeric equilibrium, thermochemical and structural properties of the electronic ground state in vacuum

For the curcuminoidic core in study, two tautomers may be formally written, keto-enolic (DPHHTO) and di-ketonic (DPHDDO) ones. Both were considered and studied at different level of the theory, and the final optimized structures are shown in Fig. 1. The two isomers present the same structural characteristics which emerged in the previous study on curcumin [10]. While the keto-enolic isomer shows a planar quasi-C_{2v} symmetric structure, the di-ketonic one assumes the typical angulated space disposition, because of the presence of a tetrahedral carbon, with the two carbonylic groups pointing to opposite senses, in order to minimize the total molecular electrostatic dipole moment.

Calculated values for DPHHTO and DPHDDO structures are reported in Table 1. From Table 1, it emerges that MP4 and CCSD methodologies give similar results, which are systematically higher than DFT ones. Nevertheless, the relative differences for the two tautomers do not change

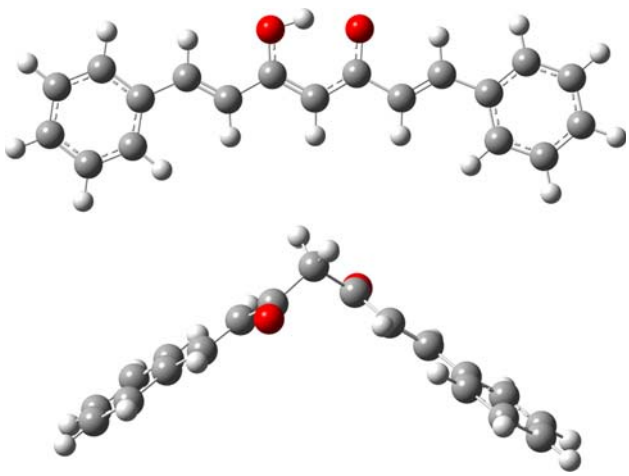

Fig. 1 The final optimized structures of the electronic ground state of DPHHTO (*top*) and of DPHDDO (*bottom*) at B3LYP/6-311g(p,d) level

Table 1 The total electronic energies E and their relative differences, for the electronic ground state of DPHHTO and of DPHDDO, in vacuum, at different levels of the theory

	$E^{(\mathrm{DPHHTO})a}$	$E^{(\mathrm{DPHDDO})a}$	ΔE^b
b3lyp/6-311g(*d*,*p*)[c]	−884.316798	−884.305166	7.30
b3lyp/6-311++g(3*df*,3*pd*)[c]	−884.395977	−884.383036	8.12
b3lyp/lanl2dz[c]	−883.965398	−883.951310	8.84
b3lyp/dgtzvp[c]	−884.141177	−884.127680	8.47
b3lyp/aug-cc-pv6z[c]	−884.401873	−884.388921	8.13
mp4(sdtq)/6-311g(*d*,*p*)[d]	−880.763446	−880.753091	6.50
mp4(sdtq)/6-311 ++g(3*df*,3*pd*)[d]	−880.810323	−880.798690	7.30
mp4(sdtq)/lanl2dz[d]	−880.279400	−880.265854	8.50
mp4(sdtq)/dgtzvp[d]	−880.479595	−880.466849	8.00
mp4(sdtq)/aug-cc-pv6z[d]	−880.855121	−880.843455	7.32
ccsd(t,e4t)/6-311g(*d*,*p*)[d]	−880.761203	−880.750715	6.58
ccsd(t,e4t)/6-311++g(3*df*,3*pd*)[d]	−880.809172	−880.797519	7.31
ccsd(t,e4t)/lanl2dz[d]	−880.279478	−880.265905	8.52
ccsd(t,e4t)/dgtzvp[d]	−880.479621	−880.466792	8.05
ccsd(t,e4t)/aug-cc-pv6z[d]	−880.855034	−880.843345	7.33

[a] In hartree

[b] In kcal mol^{-1}, $\Delta E \equiv E^{(\mathrm{DPHDDO})} - E^{(\mathrm{DPHHTO})}$

[c] With geometry optimization

[d] Without geometry optimization (single point on the respective optimized geometry)

Table 2 The total electronic energies E, with zero point vibrational energies $E + \hbar\omega/2$,Gibbs free energies G, enthalpies H and their relative differences, at DFT B3-LYP/6-311g(*d*,*p*) level, for the electronic ground state of DPHHTO and of DPHDDO, in vacuum, at $T = 298.150$ K

	E^a	$(E + \hbar\omega/2)^a$	G^a	H^a
DPHHTO	−884.316798	−884.020847	−884.070705	−884.001821
DPHDDO	−884.305166	−884.009873	−884.062272	−883.990299
	ΔE^b	$\Delta(E + \hbar\omega/2)^b$	ΔG^b	ΔH^b
DPHHTO	0	0	0	0
DPHDDO	7.30	6.89	5.29	7.23

[a] In hartree

[b] In kcal mol^{-1}

remarkably. As for curcumin [10], keto-enolic form results decidedly more stable than di-ketonic one, because of the preserved conjugated system. The average ΔE of the values as obtained as having employed different computational approaches is about 7.75 kcal mol^{-1}, which is in reasonably good agreement with the DFT B3-LYP/6-311g(*d*,*p*) value. Therefore, the DFT B3-LYP/6-311g(*p*,*d*) approach shows a logical reliability for the description of the tautomeric equilibrium. In order to contain the computational costs, consequently this approach may be chosen as theory level for the successive calculations. The energy difference between the two tautomers is so important that the presence of DPHDDO at room temperature may be neglected. Actually, its Boltzmann's factor at $T = 298.150$ K is about 4.5×10^{-6}. Such large energy difference does not occur only considering the total electronic energy, but also referring to all the calculated thermodynamical parameters at DFT B3-LYP/6-311g(*d*,*p*) level of the theory as reported in Table 2.

Another confirmation of the experimental presence of DPHHTO is provided by the comparison of the geometrical parameters between the final optimized structure and the crystallographic X-ray data [21]. In Table 3, calculated and experimental bond lengths between heavy atoms are reported. A very good agreement emerges, actually all calculated values fall in the experimental ranges.

Using both theoretical and experimental data, bond length alternation (BLA) values were evaluated, which are $\mathrm{BLA}^{(\mathrm{calc.})} = 0.103$ Å, $\mathrm{BLA}^{(\mathrm{exp.})} \sim 0.104(6)$ Å. They were calculated according to the following formula:

$$\mathrm{BLA} = \frac{1}{3}\left[\left(\frac{a+h}{2} + c + f\right) - \left(b + \frac{d+e}{2} + g\right)\right],$$

where $a \equiv \bar{b}(\mathrm{C}(6) - \mathrm{C}(7))$, $b \equiv \bar{b}(\mathrm{C}(7) - \mathrm{C}(8))$, $c \equiv \bar{b}(\mathrm{C}(8) - \mathrm{C}(9))$, $d \equiv \bar{b}(\mathrm{C}(9) - \mathrm{C}(10))$, $e \equiv \bar{b}(C(10) - C(11))$, $f \equiv \bar{b}(\mathrm{C}(11) - \mathrm{C}(12))$, $g \equiv \bar{b}(\mathrm{C}(12) - \mathrm{C}(13))$ and h $h \equiv \bar{b}(\mathrm{C}(13) - \mathrm{C}(14))$, referring to Scheme 1b. The obtained BLA values for DPHHTO are similar, even if

Table 3 Comparison between calculated and experimental bond lengths for the electronic ground state of DPHHTO in vacuum

Distance	Calc.	Exp.[a]	Distance	Calc.	Exp.[a]
C(1)–C(2)	1.391	1.388 (5)	C(2)–C(3)	1.389	1.385 (6)
C(3)–C(4)	1.398	1.401 (6)	C(4)–C(5)	1.381	1.379 (6)
C(5)–C(6)	1.400	1.398 (5)	C(6)–C(1)	1.408	1.410 (5)
C(6)–C(7)	1.475	1.478 (5)	C(7)–C(8)	1.347	1.345 (6)
C(8)–C(9)	1.467	1.469 (6)	C(9)–C(10)	1.405	1.406 (6)
C(10)–C(11)	1.403	1.407 (6)	C(11)–C(12)	1.475	1.477 (6)
C(12)–C(13)	1.349	1.353 (6)	C(13)–C(14)	1.461	1.466 (5)
C(14)–C(15)	1.397	1.395 (5)	C(15)–C(16)	1.387	1.382 (6)
C(16)–C(17)	1.407	1.406 (6)	C(17)–C(18)	1.380	1.383 (6)
C(18)–C(19)	1.391	1.385 (6)	C(19)–C(14)	1.405	1.413 (5)
C(9)–O(20)	1.305	1.302 (5)	C(11)–O(21)	1.296	1.294 (5)

All values are in Ångstrøm. Atoms numeration refers to Scheme 1. Estimated standard deviations in parentheses

[a] From Ref. [6]

larger, with respect to those for curcumin in vacuum at DFT level [9].

Table 4 collects and compares calculated and experimental bond angles formed by heavy atoms. Even for these geometrical parameters, a good agreement may be appreciated.

Instead, a comparison between calculated and experimental dihedral angles for the electronic ground state of DPHHTO shows the theoretical structure almost flat, and so more planar than the X-ray provided one, which suggests deviations from the planarity till 10°/12° for some angles. Such evidence might be caused by the interaction of the molecule with the near neighbours in the crystal. However, torsional angles values offer the experimental confirmation of the clearly larger stability of DPHHTO isomer with respect to DPHDDO one, at room temperature. Actually, the dihedral angles formed by O(20)–C(9)–C(10)–C(11) and C(9)–C(10)–C(11)–O(21) atoms (see Scheme 1b), which crystallographic study [21] gives of −2.1(6)° and 2.7(6)° respectively, are closer to the values found for the final optimized geometry of DPHHTO (both nulls) than those of DPHDDO (101.3° and 106.0°, respectively). Therefore, the reference of the authors of [21] to the studied structure as DPHDDO must be considered as a venial misunderstanding. On the basis of what above said, all the following results regard DPHHTO, if not differently specified.

The present tautomeric study on the electronic ground state of DPHHTO concludes with the analysis of the influence on the total energy of the value of the two phenyls dihedral angles. In Table 5, results concerning energy differences between the structures as obtained modifying the two phenyls dihedral angles values and the final optimized geometry are reported. On the basis of such data, Boltzmann's factors are estimated at $T = 298.150$ K and collected in Table 6. Two main remarks may be evinced. First, only structures which have both dihedral angles within the values of 30° are appreciably accessible at the considered temperature. The other interesting evidence concerns the different effect that the same imposed value to the two dihedral angles provides. Evidently, although from a geometrical point of view the molecule appears as quasi perfectly C_{2v} symmetrical, the effects of the larger conjugation in the closest moiety to enolic group are noticeable.

3.2 Electronic properties and UV–Vis spectrum in vacuum

During the presentation of the results and their following discussions, as well as the classification of configurations,

Table 4 Comparison between calculated and experimental bond angles for the electronic ground state of DPHHTO in vacuum

Angle	Calc.	Exp.[a]	Angle	Calc.	Exp.[a]
C(1)–C(2)–C(3)	120.1	120.4 (4)	C(2)–C(3)–C(4)	119.5	119.5 (4)
C(3)–C(4)–C(5)	120.3	120.0 (4)	C(4)–C(5)–C(6)	121.1	121.5 (4)
C(5)–C(6)–C(1)	118.0	117.9 (4)	C(6)–C(1)–C(2)	120.9	120.7 (4)
C(1)–C(6)–C(7)	118.4	118.3 (4)	C(5)–C(6)–C(7)	123.6	123.8 (4)
C(6)–C(7)–C(8)	127.5	127.0 (4)	C(7)–C(8)–C(9)	122.3	122.1 (4)
C(8)–C(9)–C(10)	120.4	120.9 (4)	C(9)–C(10)–C(11)	120.6	120.2 (4)
C(10)–C(11)–C(12)	120.9	121.0 (4)	C(11)–C(12)–C(13)	122.1	122.2 (4)
C(12)–C(13)–C(14)	128.1	127.8 (4)	C(13)–C(14)–C(15)	123.3	123.7 (4)
C(14)–C(15)–C(16)	121.1	121.6 (4)	C(15)–C(16)–C(17)	120.2	119.9 (4)
C(16)–C(17)–C(18)	119.2	119.3 (4)	C(17)–C(18)–C(19)	120.6	120.6 (4)
C(18)–C(19)–C(14)	121.0	120.8 (4)	C(19)–C(14)–C(15)	117.9	117.7 (4)
C(13)–C(14)–C(19)	118.7	118.4 (4)			
C(8)–C(9)–O(20)	119.1	118.5 (4)	O(20)–C(9)–C(10)	120.5	120.6 (4)
C(10)–C(11)–O(21)	121.3	121.3 (4)	O(21)–C(11)–C(12)	117.8	117.6 (4)

All values are in degrees. Atoms numeration refers to Scheme 1. Estimated standard deviations in parentheses

[a] From Ref. [6]

Table 5 Energy differences, in kcal mol^{-1}, between the modified geometries and the final optimized one

	ΔE						
	$\delta_2 = 0°$	$\delta_2 = 15°$	$\delta_2 = 30°$	$\delta_2 = 45°$	$\delta_2 = 60°$	$\delta_2 = 75°$	$\delta_2 = 90°$
$\delta_1 = 0°$	0	0.18	0.95	2.29	3.99	5.38	5.97
$\delta_1 = 15°$	0.19	0.40	1.17	2.51	4.25	5.62	6.14
$\delta_1 = 30°$	0.97	1.20	1.93	3.26	4.96	6.36	6.94
$\delta_1 = 45°$	2.32	2.53	3.27	4.64	6.31	7.73	8.34
$\delta_1 = 60°$	4.03	4.28	4.98	6.32	7.99	9.41	10.05
$\delta_1 = 75°$	5.44	5.67	6.38	7.74	9.40	10.83	11.47
$\delta_1 = 90°$	6.02	6.19	6.96	8.36	10.04	11.46	12.06

Dihedral angles are defined $\delta_1 \equiv$ C(5)–C(6)–C(7)–C(8) and $\delta_2 \equiv$ C(12)–C(13)–C(14)–C(15), where atoms numeration refers to Scheme 1

Table 6 Boltzmann's factors for the energies values of Table 5, at $T = 298.150$ K

	ΔE						
	$\delta_2 = 0°$	$\delta_2 = 15°$	$\delta_2 = 30°$	$\delta_2 = 45°$	$\delta_2 = 60°$	$\delta_2 = 75°$	$\delta_2 = 90°$
$\delta_1 = 0°$	1	7.3462E-01	2.0045E-01	2.0991E-02	1.1968E-03	1.1312E-04	4.2094E-05
$\delta_1 = 15°$	7.2779E-01	5.0761E-01	1.3805E-01	1.4544E-02	7.7078E-04	7.5368E-05	3.1300E-05
$\delta_1 = 30°$	1.9314E-01	1.3294E-01	3.8555E-02	4.0487E-03	2.3170E-04	2.1920E-05	8.1889E-06
$\delta_1 = 45$	2.0012E-02	1.3936E-02	3.9965E-03	3.9629E-04	2.3641E-05	2.1658E-06	7.6332E-07
$\delta_1 = 60°$	1.1039E-03	7.2395E-04	2.2499E-04	2.3279E-05	1.3980E-06	1.2731E-07	4.3235E-08
$\delta_1 = 75°$	1.0354E-04	6.9678E-05	2.1125E-05	2.1349E-06	1.2838E-07	1.1580E-08	3.9162E-09
$\delta_1 = 90°$	3.8851E-05	2.8822E-05	7.8951E-06	7.4991E-07	4.3484E-08	3.9455E-09	1.4315E-09

Dihedral angles are defined as in Table 5

Table 7 Eigenvalues (in eV) corresponding to $H - 2$, $H - 1$, H, L, $L + 1$ and $L + 2$ MOs of DPHHTO (a) and DPHDDO (b), as calculated at CS INDO and DFT B3LYP/6-311g(p,d) level

	CS INDO						DFT	
	SL		OK		MN		B3LYP/6-311g(p,d)	
	(a)	(b)	(a)	(b)	(a)	(b)	(a)	(b)
$H - 2$	−0.4188	−0.4263	−0.3859	−0.3951	−0.3491	−0.3546	−0.2605	−0.2487
$H - 1$	−0.3785	−0.3924	−0.3587	−0.3667	−0.3198	−0.3249	−0.2413	−0.2440
H	−0.3690	−0.3920	−0.3371	−0.3647	−0.2978	−0.3228	−0.2223	−0.2432
L	−0.0054	0.0081	−0.0387	−0.0335	−0.0711	−0.0624	−0.0941	−0.0905
$L + 1$	0.0275	0.0149	−0.0014	−0.0222	−0.0286	−0.0494	−0.0567	−0.0758
$L + 2$	0.0558	0.0578	0.0267	0.0270	−0.0015	−0.0008	−0.0202	−0.0219

SL Slater theoretical integrals, *OK* Ohno-Klopman spectroscopic parameterization, *MN* Mataga-Nishimoto spectroscopic parameterization

the frontier orbitals HOMO and LUMO will be indicated with H and L, respectively.

Table 7 collects the eigenvalues corresponding to $H - 2$, $H - 1$, H, L, $L + 1$ and $L + 2$ MOs of DPHHTO and DPHDDO, as calculated at CS INDO (with different integrals evaluations) and DFT B3LYP/6-311g(p,d) level. Although the absolute energy values obtained with different methodologies are dissimilar, some general considerations may be evinced. Occupied MOs energies of DPHHTO are always higher than DPHDDO ones, and for both DPHHTO and DPHDDO the energy order $\varepsilon_i^{(SL)} < \varepsilon_i^{(OK)} < \varepsilon_i^{(MN)} < \varepsilon_i^{(DFT)}$ is respected for each ith occupied MO (calculated at the different levels), while the opposite for virtual MOs, so also positive energy values are obtained with Slater and Ohno-Klopman integral for CS INDO calculations. Such behaviour is comprehensive of the fact that, as well known [22–25], Mataga-Nishimoto parameterization introduces an appreciable quantity of electronic correlation into the SCF procedure yet. Such correlation effects are introduced in less measure with Ohno-Klopman parameterization and, instead,

are excluded by employing Slater's orbitals. As well as pointed out for curcumin [10], $H-1$ and H are almost degenerate for diketo-tautomer.

Considering the eigenvalues differences, for instance with respect to H in case of occupied MOs and with respect to L in case of virtual MOs, the description is not quantitatively dissimilar in the case of the different calculation methods, for both occupied and unoccupied MOs. In general, as consequence of what above reported, the energy differences between MOs are larger in the case of the keto-enolic isomer, with respect to the di-ketonic one. Actually, in the case of DPHHTO (and DPHDDO), $\Delta\varepsilon_{H,H-2} \sim -0.05$ (-0.03) eV for CS INDO and ~ -0.04 (-0.01) eV for DFT results, and $\Delta\varepsilon_{H,H-1} \sim -0.02$ eV and ~ -0.01 eV with Slater integrals. Concerning virtual MOs, instead, in the case of DPHHTO (and DPHDDO), $\Delta\varepsilon_{L,L+1}$ and $\Delta\varepsilon_{L,L+2}$ respectively result ~ 0.04 (0.01) eV and ~ 0.07 (0.06) eV, as its place ~ 0.03 (0.01) eV and ~ 0.06 (0.05) eV with Slater integrals. The eigenvalues and their relative differences, as calculated at DFT B3LYP/6-311g(p,d) level, are quite dissimilar with regard to those obtained for curcumin tautomers with the same computational method [10].

Figure 2 shows the representations of $H-2$, $H-1$, H, L, $L+1$ and $L+2$ MOs densities, as calculated for both DPHHTO and DPHDDO optimized structures, at B3LYP/6-311 g(p,d) level. Concerning DPHHTO, $H-1$, H, L and $L+1$ are delocalized on the entire molecule, being the electronic density distributed both on the dienic and on the benzenic moiety of the molecule, while $H-2$ is localized on the central part and $L+2$ on one benzenic ring, as well as $L+3$ (not shown) on the other one. Regarding DPHDDO, similarly to DPHHTO, $H-2$ is localized on the central part of the molecule, while L and $L+1$ are delocalized on the entire molecule. Instead, $H-1$ and H, which are quasi-degener (as above said), result delocalized on the two half molecule. About $L+2$ and $L+3$ (not

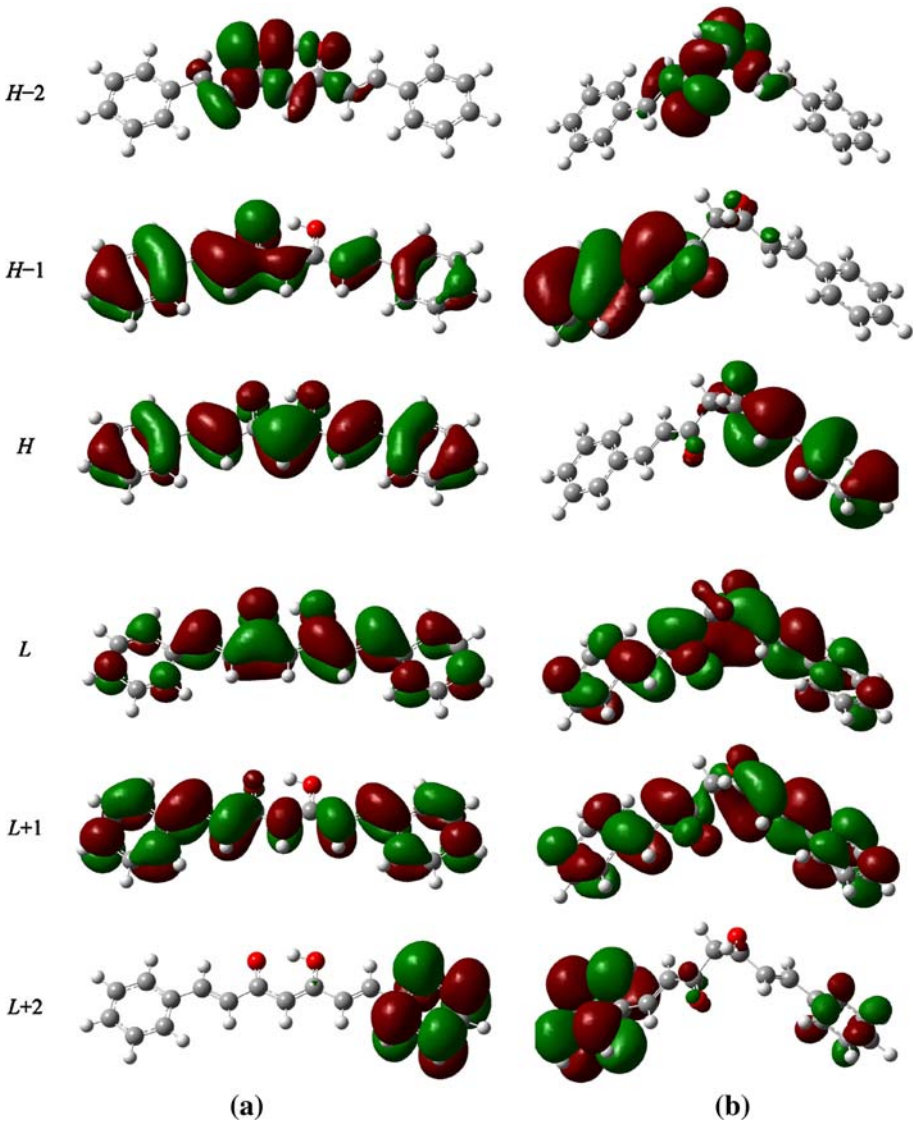

Fig. 2 Representations of $H-2$, $H-1$, H, L, $L+1$ and $L+2$ MOs densities of DPHHTO (**a**) and DPHDDO (**b**), at B3LYP/6-311g(p,d) level (isovalue $\phi = 0.2$)

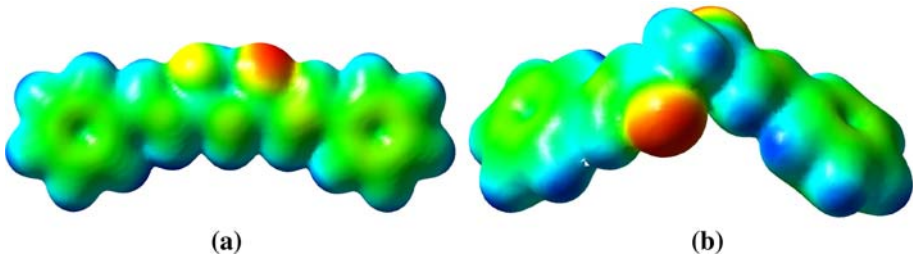

Fig. 3 Molecular electrostatic maps of DPHHTO (**a**) and of DPHDDO (**b**) at B3LYP/6-311g(*p*,*d*) level (isovalue $\phi = 0.05$)

shown), an analogy with the correspondent MOs of DPHHTO may be seen, i.e. they are localized on the benzenic part of the molecule, even if in this case a smaller component also on the other benzene and on the nearest carbonylic group is present. An analogous behaviour was pointed out for curcumin [10].

For the two ground states optimized structures of Fig. 1, molecular electrostatic maps (MEPs) were calculated. Results are shown in Fig. 3. For both DPHHTO and DPHDDO the negative charge is localized on the oxygen atoms. While for DPHDDO the two oxygen atoms show the same charge, for DPHHTO the hydrogen bounded oxygen is less negative with respect to the carbonylic one because of the partial charge delocalization along the bound with hydrogen.

Because of its so scarce presence at room temperature, DPHDDO spectroscopic properties were not calculated. In Table 8 results on $S_0 \rightarrow S_n$ ($n = 1, 2,\ldots, 8$) absorption spectra of DPHHTO in vacuum are reported, as obtained at CI-S DFT, at TD-DFT and at CS INDO SDT-CI level. From a previous work [9], it emerged that CS INDO SDT-CI method provides the best description of the electronic absorption spectrum of curcumin. In this case, in absence of an experimental reference, such calculations will be used as comparison for the ab initio results. While TD-DFT spectrum is very similar to CS INDO one, even if lightly red shifted for the first transitions, the CI-S calculation deals to a different description. In fact, it is remarkably blue shifted and the relative transitions intensities are dissimilar with respect to the two other models. Moreover, it is interesting to underline the inversion of the second and the third excited states.

The TD-DFT and CS INDO wave functions which describe the selected singlet excited states are very similar to those illustrated for curcumin [9]. Also for DPHHTO, the enclosure of doubly-excited configurations is an aspect of crucial importance in order to correctly describe the states composition, as emerged for curcumin, especially for $|S_n\rangle$ ($n > 4$) states. The first singlet excited state is mainly characterized by the single-excited $|H\,L\rangle$ and $|H-1\,L+1\rangle$ configurations and the double-excited $\left|H^0\,L^2\right\rangle$ configuration. The second and the third states result inverted with respect to curcumin. For the higher states, the double-excited $\left|H^0\,L^2\right\rangle$, $\left|H^0\,L, L+1\right\rangle$ and $\left|H-1, H\,L^2\right\rangle$ configurations hold a decisive relevance.

3.3 Electronic singlet excited states optimized structures of DPHHTO in vacuum

First of all, some general considerations of comparison between the three adopted methodologies may be exposed. While TD-DFT and CAS-SCF provided analogous geometries and qualitatively similar results, with CI-S method a significantly different picture was reached. Through TD-DFT and CAS-SCF, an appreciable structural differentiation was shown for the excited states geometries, instead CI-S does not dealt remarkably different geometries with respect to the ground state one. Moreover, CAS-SCF gave structures with no negative frequencies values, while a high incidence of imaginary vibrations was found

Table 8 Results on $S_0 \rightarrow S_n$ ($n = 1, 2,\ldots, 8$) absorption spectra of DPHHTO in vacuum

	CI-S			TD-DFT			CS INDO SDT-CI		
	ΔE (eV)	λ (nm)	f	ΔE (eV)	λ (nm)	f	ΔE (eV)	λ (nm)	f
$S_0 \rightarrow S_1$	4.325736	286.62	2.2519	3.208536	386.42	1.4547	3.331835	372.12	1.5974
$S_0 \rightarrow S_2$	5.162998	240.14	0.0901	3.406254	363.99	0.0008	3.454755	358.88	0.0015
$S_0 \rightarrow S_3$	5.328072	232.70	0.0000	3.730757	332.33	0.0462	3.764285	329.37	0.1212
$S_0 \rightarrow S_4$	5.728342	216.44	0.0055	4.160545	298.00	0.0011	6.279591	297.44	0.0074
$S_0 \rightarrow S_5$	5.743734	215.86	0.0087	4.202001	295.06	0.0074	4.205850	294.79	0.0277
$S_0 \rightarrow S_6$	5.864357	211.42	0.0072	4.227504	293.28	0.0051	4.229668	293.13	0.0095
$S_0 \rightarrow S_7$	6.617434	187.36	0.2844	4.369797	283.73	0.1293	4.373033	283.52	0.1124
$S_0 \rightarrow S_8$	6.941618	178.61	0.3053	4.706177	263.45	0.3252	4.712975	263.07	0.2871

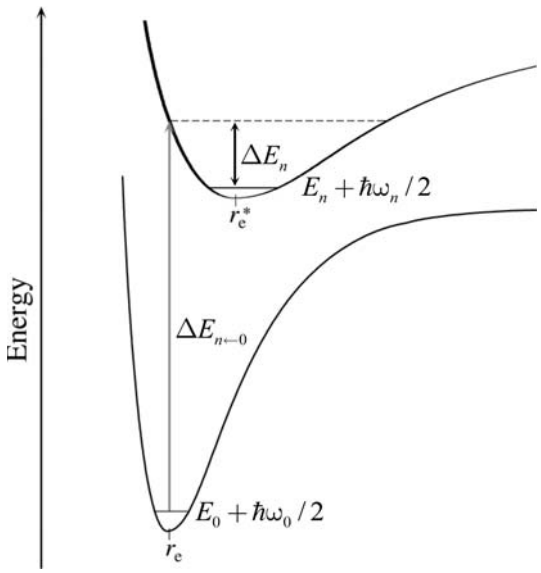

Fig. 4 Simplified representation of the electronic ground state's potential energy hyper-surfaces two-dimensional sections and of an electronic bond excited state's one

for CI-S geometries, especially for higher energy ones. For these reasons, following, only CAS-SCF results will be presented and discussed. A qualitative comparison with TD-DFT outputs will be also mentioned.

In order to introduce the adopted notation, in Fig. 4 a simplified representation of the electronic ground state's potential energy hyper-surfaces two-dimensional section and of an electronic bond excited state's one is shown. Total electronic energies corrected with zero point vibrational energy of the ground ($n = 0$) and of the nth excited state, the transition energy and the vibrational deactivation energy are respectively indicated with $(E_n + \hbar\omega_n/2)$, $\Delta E_{n\leftarrow 0}$ and ΔE_n.

The above-mentioned energies represent an important aspect for the present study. Table 9 collects such values for the first eight singlet excited states for CAS-SCF calculations, while Scheme 2 provides a visual representation. Some interesting aspects may be evinced by the values reported in Table 9. As a consequence of the excitation to S_4, S_5 and S_6 states, very close energy conditions are reached. ΔE_n values vary from $\sim$15.8 kcal mol^{-1} (for S_1) to $\sim$31.1 kcal mol^{-1} (for S_7). In particular, the highest ΔE_n values were obtained for S_5 and S_7. On the basis of ΔE_n values, the considered states may be classified into three groups: in increasing order, (1) S_1 and S_6; (2) S_2, S_3, S_4 and S_8; (3) S_5 and S_7. Such evidence, combined with the close energy values for S_4, S_5 and S_6 states, causes an inversion in the order of states when the total energies $(E_n + \hbar\omega_n/2)$ of the optimized structures are considered (Scheme 2).

This may induce to consider the presence of intersections between the potential energy hyper-surfaces. After

Table 9 Singlet excited states S_n ($n = 1, 2,\ldots, 8$) energies of DPHHTO (CAS-SCF)

S_n	$[(E_0 + \hbar\omega_0/2) + \Delta E_{n\leftarrow 0}]^a$	$(E_n + \hbar\omega_n/2)^a$	ΔE_n^b
$n = 0$	–	−884.020847	–
1	−883.902936	−883.928179	15.84
2	−883.895670	−883.926300	19.22
3	−883.883744	−883.917457	21.15
4	−883.867950	−883.897899	18.79
5	−883.866426	−883.913221	29.36
6	−883.865489	−883.892838	17.16
7	−883.860260	−883.909822	31.10
8	−883.847898	−883.880071	20.19

[a] In hartree

[b] In kcal mol^{-1}

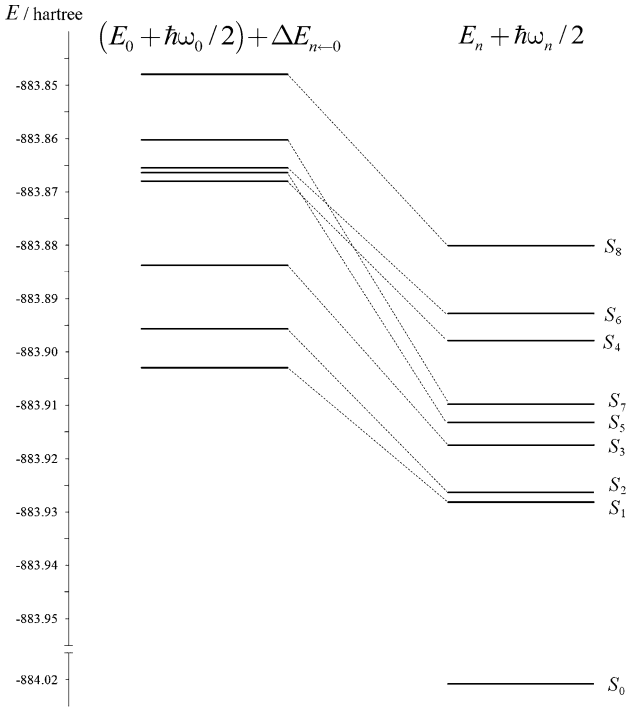

Scheme 2 Energy levels of singlet excited states S_n ($n = 1,\ldots, 8$) with respect to the ground state S_0, after vertical transitions (*left side*) and after relaxations (*right side*)

the full geometry optimization, S_5 crosses S_4, while S_7 crosses both S_4 and S_6, and the close energy gap between S_4, S_5 and S_6 becomes wider. The opposite happens to S_1 and S_2, whose gaps are $\sim$4.6 kcal mol^{-1} before and $\sim$1.2 kcal mol^{-1} after the optimizations. This means that, if S_1 and S_2 life times are long enough, populating the first singlet state, an ineligible thermal population also of the second state should be observable at room temperature (about 13.67% at 298.150 K).

Considerations on the energies have important counterparts on the geometrical aspects. About the structures of the singlet excited states S_n ($n = 1, 2,\ldots, 8$) optimized

Table 10 Some remarkable geometrical parameters' values for the singlet excited states S_n ($n = 1, 2,\ldots, 8$) optimized geometries (CAS-SCF)

	S_1	S_2	S_3	S_4	S_5	S_6	S_7	S_8
Interatomic distances (Å)								
C(9)–C(10)	1.362	1.355	1.343	1.353	1.406	1.364	1.452	1.343
C(10)–C(11)	1.449	1.452	1.464	1.456	1.432	1.462	1.452	1.463
C(9)–O(20)	1.325	1.317	1.342	1.320	1.322	1.349	1.317	1.342
C(11)–O(21)	1.236	1.221	1.261	1.227	1.241	1.236	1.317	1.260
O(20)–H	0.959	0.960	0.944	0.962	1.061	0.966	1.734	0.944
O(21)–H	1.783	2.259	2.051	1.753	1.386	1.793	1.903	2.049
Bond angles (°)								
C(9)–C(10)–C(11)	122.4	135.0	127.2	121.8	106.3	121.9	134.9	127.1
C(10)–C(9)-O(20)	122.9	123.1	125.4	123.1	120.7	123.9	116.4	125.3
C(10)–C(11)-O(21)	121.7	122.0	119.6	121.4	121.6	120.8	122.1	119.6
Dihedral angles (°)								
C(5)–C(6)–C(7)–C(8)	0.0	0.0	0.0	0.0	18.2	12.0	0.0	27.5
C(7)–C(8)–C(9)–C(10)	−180.0	−152.0	−180.0	−180.0	−180.0	−145.1	−151.9	179.8
C(10)–C(11)–C(12)–C(13)	−180.0	−152.0	−180.0	−180.0	−180.0	−162.0	−149.7	176.2
C(12)–C(13)–C(14)–C(15)	0.0	0.0	0.0	0.0	18.4	3.4	0.0	27.5
C(9)–C(10)–C(11)–O(21)	0.0	0.0	0.0	0.0	37.4	2.6	45.8	4.0
O(20)–C(9)–C(10)–C(11)	0.0	0.0	0.0	0.0	0.0	1.5	44.7	0.0

geometries, some remarkable parameters values obtained with CAS-SCF methodology are reported in Table 10, while Fig. 5 shows pictures of such structures. All the geometries are bond structures and no negative frequencies are found in the vibrational spectrum ("genuine" minima were reached).

Comparing the values of Table 10 with those of Tables 3 and 4, the optimized geometries may be grouped into two classes: on one hand, the first four lowest energy states geometries, which present very similar characteristics with respect to the ground state one, and the other hand, the four highest energy states ones, which remarkably differ from the ground state one. In particular, the most important structural changes are visible for S_5 and S_7 geometries.

Concerning the first four structures, they look very similar each other and to the ground state one. In particular, the first, the third and the fourth may be considered not substantially different each other. Instead, the second excited state geometry presents some diversity, specifically regarding the wider central bond angle, which is also the largest if compared with all the structures, and the deviation from the planarity caused by the two non-flat dihedral angles. Another aspect which communizes these structures is the high symmetry level. Similar results were obtained also with TD-DFT method.

The last four geometries, instead, are characterized by important geometrical modifications, especially involving the central moiety and the dihedral angles. S_6 and S_8 geometries look quite similar to those of the first four singlet excited states, even if the deviation from the planarity is more appreciable. On the contrary, the case of S_5 and S_7 geometries is significantly different. Comparing S_5 geometry with ground state one, a remarkable decrease of the central bond angle and the planarity loss are the most salient characteristics. All the other parameters remain roughly unchanged, with exception of the alcoholic hydrogen approaching to the carbonylic oxygen. Undoubtedly, one of the most interesting obtained geometries is represented by S_7 one. Such significance is also increased, because, as emerged from spectral study, the transition from the ground state to the seventh singlet excited state is a medium intensity one. From a geometrical point of view, the two bond lengths C(9)–C(10) and C(10)–C(11) and the two bond lengths C(9)–O(20) and C(11)–O(21) are exactly the same, and the alcoholic hydrogen appears in an intermediate position, unbounded with both the oxygens. Because the two oxygen atoms deviate from the local plain into opposite sides, in the central region the molecule looks widely opened. In its totality, the structure seems quite symmetrical, also considering the dihedral angles, which confer a corrugated aspect to DPHHTO in this state.

Table 11 collects the eigenvalues corresponding to $H - 2$, $H - 1$, H, L, $L + 1$ and $L + 2$ MOs, as calculated for singlet excited states S_n ($n = 1, 2,\ldots, 8$) optimized geometries (CAS-SCF), at B3LYP/6-311g(p,d) level. In spite of ground state, in this case CS INDO eigenvalues are not reported because they were not involved during the optimization jobs. Although some dissimilarities involving

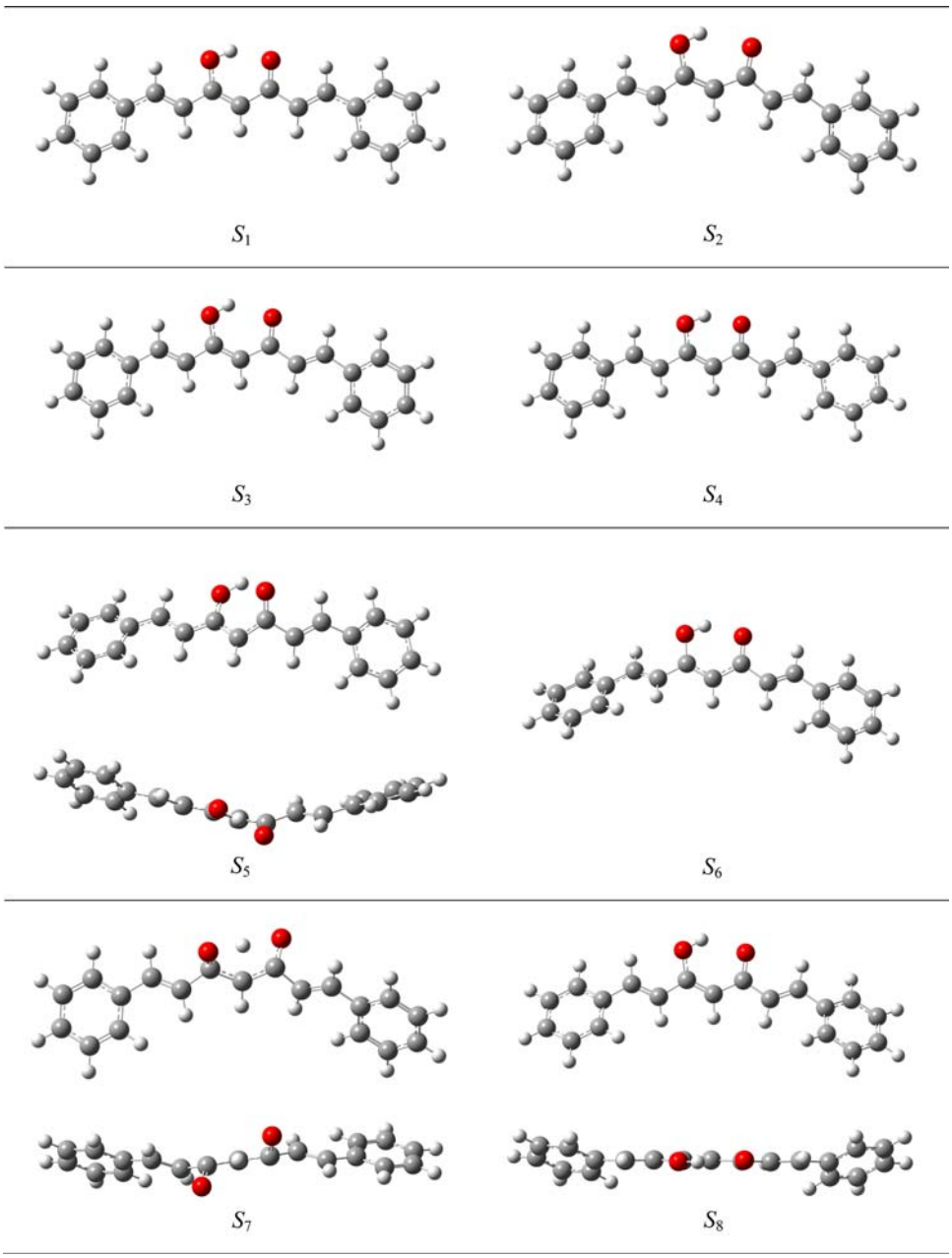

Fig. 5 Pictures of singlet excited states S_n ($n = 1, 2,\ldots, 8$) optimized geometries (CAS-SCF), at B3LYP/6-311g(p,d) level

Table 11 Eigenvalues (in eV corresponding to $H - 2$, $H - 1$, H, L, $L + 1$ and $L + 2$ MOs, as calculated for singlet excited states S_n ($n = 1, 2,\ldots, 8$) optimized geometries (CAS-SCF), at B3LYP/6-311g(p,d) level

MOs	S_1	S_2	S_3	S_4	S_5	S_6	S_7	S_8
$H - 2$	−0.2534	−0.2552	−0.2501	−0.2584	−0.2488	−0.2566	−0.2470	−0.2521
$H - 1$	−0.2384	−0.2351	−0.2417	−0.2406	−0.2410	−0.2401	−0.2389	−0.2429
H	−0.2255	−0.2196	−0.2250	−0.2235	−0.2101	−0.2240	−0.2235	−0.2273
L	−0.0844	−0.0941	−0.0923	−0.0916	−0.0956	−0.0880	−0.1095	−0.0912
$L + 1$	−0.0515	−0.0593	−0.0535	−0.0550	−0.0597	−0.0548	−0.0906	−0.0499
$L + 2$	−0.0186	−0.0169	−0.0179	−0.0233	−0.0176	−0.0199	−0.0515	−0.0175

the absolute values are notable (in particular referring to S_5 and S_7), with respect to the correspondent eigenvalues for DPHHTO ground state (Table 7), the energy differences are generally very scarce (under 0.01 eV, with exception for virtual MOs of the seventh state, which are more stable of ~ -0.02 and ~ -0.03 eV with regard to virtual MOs of the ground state). S_4 and S_6 are the states which show the closest eigenvalues referring to ground state.

As for the ground state, the eigenvalues differences with respect to H in case of occupied MOs and with respect to L in case of virtual MOs were calculated. Such gaps are quite similar for all the states. Actually, for occupied MOs, $\Delta\varepsilon_{H,H-2} \sim -0.04$ eV (S_0, S_2 and S_5), ~ -0.03 eV (S_1, S_3, S_4 and S_6) or ~ -0.02 eV (S_7 and S_8), and $\Delta\varepsilon_{H,H-1} \sim -0.03$ eV (S_5), ~ -0.02 eV (S_0, S_2, S_3, S_4, S_6, S_7 and S_8) or ~ -0.01 eV (S_1), while for unoccupied MOs, $\Delta\varepsilon_{L,L+1} \sim 0.02$ eV (S_7), ~ 0.03 eV (S_1, S_2 and S_6) or ~ 0.04 eV (S_0, S_3, S_4, S_5 and S_8), and $\Delta\varepsilon_{L,L+2} \sim 0.06$ eV (S_7), ~ 0.07 eV (S_2 and S_5) or ~ 0.08 eV (S_0, S_1, S_3, S_4, S_6 and S_8).

Figure 6 shows that strong similarities are detectable in the representations corresponding to $H-2$, $H-1$, H, L, $L+1$ and $L+2$ MOs densities for S_n ($n \neq 5, 7$) states with respect to the ground state, as happens from a structural point of view. Concerning these states, the differences refer principally to $L+2$ MOs, which sometimes are localized on both the benzenic fragments.

Rather remarkable differences regard MOs of S_5 and S_7 were found. In particular, the shapes, the localization levels and the nodal surfaces look completely modified with refer to the correspondent MOs of S_0. Such evidences support what previously said concerning the energies and the characteristics of these states.

Analogies and discrepancies with the ground state are also appreciable in MEPs (Fig. 7). Also in these cases, the negative charge is banally concentred in correspondence of the two oxygen atoms. But, while for S_n ($n \neq 5, 7$) states an analogous situation with respect to Fig. 3a is observed, in which the carbonylic oxygen shows a higher electronic density with respect to the alcoholic one, for S_5 and predominantly for S_7 a remarkable negative charge is noticeable on both the oxygen atoms. Comparing with Fig. 3, S_7 MEP provides a description which seems more similar to DPHDDO than DPHHTO, with negative charges pointing to spatially different directions and senses. Therefore, a loss of the chelant properties of curcuminoidic core is supposed, whether this excited state might be populated.

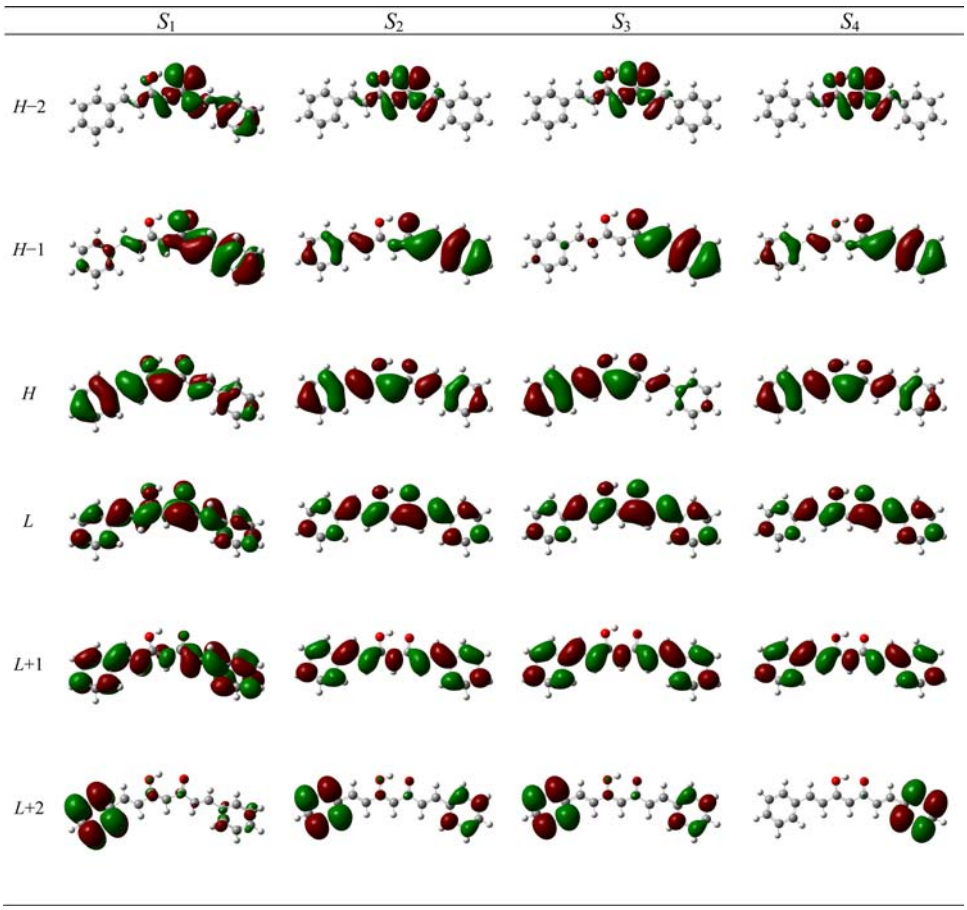

Fig. 6 Representations of $H-2$, $H-1$, H, L, $L+1$ and $L+2$ MOs densities, as calculated for singlet excited states S_n ($n = 1, 2, \ldots, 8$) optimized geometries (CAS-SCF), at B3LYP/6-311g(p,d) level (isovalue $\phi = 0.2$)

Fig. 6 continued

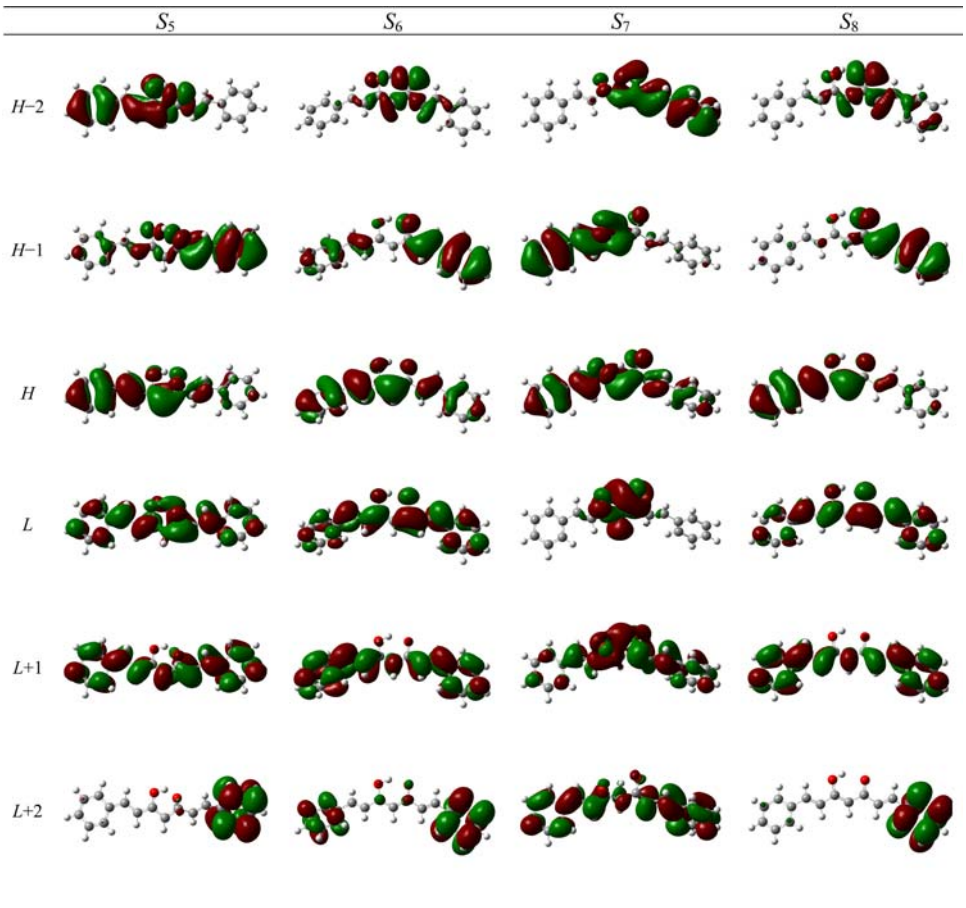

3.4 Solvent effects

With reference to the vacuum phase, the introduction of the implicit treatment of the solvent effects does not induce particularly relevant variations. Comparing values of Tables 1 and 12, a decrement in the absolute energy values is observed, similar to that said about curcumin [9]. Also relative energy differences between the two isomers DPHHTO and DPHDDO are minor, even if the general point does not significantly change, regarding the negligible presence of DPHDDO with respect to DPHHTO at $T = 298.150$ K. In other words, solvent effect is irrelevant in relation to stability and tautomeric equilibrium of DPHHTO and DPHDDO. From methanol to DMSO, energy barriers lightly decrease. For the most stable isomer, *G* and *H* values are quite similar for the two considered solvents, while a remarkable difference is shown with respect to vacuum. A small change in zero point vibrational energy is appreciable, passing from vacuum (185.71 kcal mol^{-1}), to methanol (184.13 kcal mol^{-1}), to DMSO (184.16 kcal mol^{-1}).

Concerning the ground state optimized geometry, important structural modifications are not noticeable, passing from vacuum to solvent phase. A light decrement in BLA value is shown (0.092 Å for both solvents). An explicit solvent treatment might be suggested.

In Tables 13 and 14 results on $S_0 \rightarrow S_n$ ($n = 1, 2, \ldots, 8$) absorption spectra of DPHHTO respectively in methanol and in DMSO are reported, obtained at CI-S DFT, at TD-DFT and at CS INDO SDT-CI level. As for vacuum, a good agreement is shown for TD-DFT and CS INDO SDT-CI calculation, while CI-S method provides very discordant results. This reaffirms the fundamental importance of the poly-excited configurations in the description of the electronic properties of the molecule. As for curcumin [9], the macroscopic solvent effect is a general red shift of the spectrum, which is more accentuated for DMSO (for the first and the second transition $\Delta\lambda$ are 61.60 and 63.93 nm, respectively at CS INDO level) than for methanol (38.19 and 39.75 nm), because of a larger value of the relative dielectric constant. Such effect is more noticeable on the first transitions, with different importance for the two solvents, both for energies and for intensities, and $\Delta\lambda$ is larger for CS INDO calculation than for TD-DFT (for the first transition, 29.51 and 24.84 nm, respectively in DMSO and in methanol). The shift, with respect to vacuum, is slightly more important for DPHHTO than for curcumin. The remaining of the

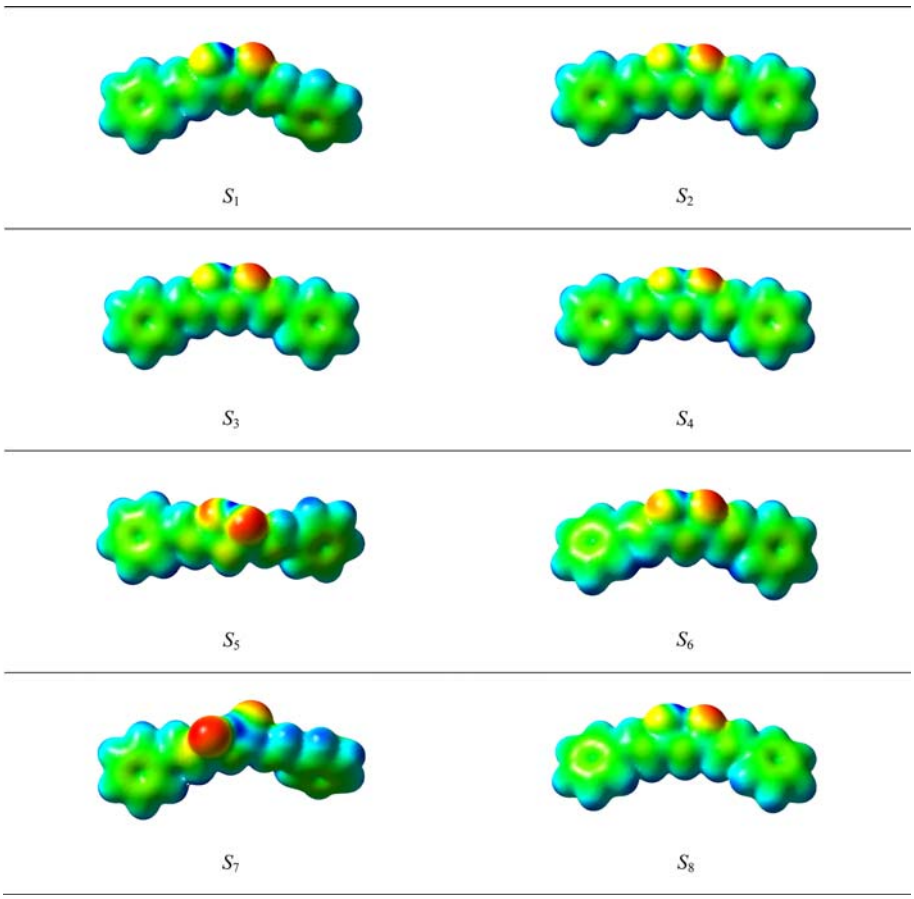

Fig. 7 Molecular electrostatic maps of singlet excited states S_n ($n = 1, 2,\ldots, 8$) optimized geometries (CAS-SCF), at B3LYP/6-311g(p,d) level (isovalue $\phi = 0.05$)

Table 12 The total electronic energies E, with zero point vibrational energies $E + \hbar\omega/2$, Gibbs free energies G, enthalpies H and their relative differences, for the electronic ground state of DPHHTO and of DPHDDO, in methanol and in DMSO, at $T = 298.150$ K

	E^a	$(E + \hbar\omega/2)^a$	G^a	H^a
Methanol				
DPHHTO	−884.337900	−884.044466	−884.094762	−884.025391
DPHDDO	−884.327926	−884.035055	−884.087834	−884.015477
DMSO				
DPHHTO	−884.337816	−884.044343	−884.094721	−884.025273
DPHDDO	−884.328065	−884.035219	−884.088101	−884.015635
	ΔE^b	$\Delta(E + \hbar\omega/2)^b$	ΔG^b	ΔH^b
Methanol				
DPHHTO	0	0	0	0
DPHDDO	6.26	5.90	4.35	6.22
DMSO				
DPHHTO	0	0	0	0
DPHDDO	6.12	5.72	4.15	6.05

[a] In hartree

[b] In kcal mol^{-1}

spectral transitions does not show particular differences between the two solvents. An interesting evidence concerns the transition $S_0 \rightarrow S_2$, which at TD-DFT level results blue shifted with respect to vacuum (for both the solvents; $\Delta\lambda = 11.26$ nm in DMSO, 10.9 nm in methanol), while with CS INDO SDT-CI method it follows the

Table 13 Results on $S_0 \rightarrow S_n$ ($n = 1, 2,\ldots, 8$) absorption spectra of DPHHTO in methanol

	CI-S			TD-SCF			CS INDO SDT-CI		
	ΔE (eV)	λ (nm)	F	ΔE (eV)	λ (nm)	f	ΔE (eV)	λ (nm)	f
$S_0 \rightarrow S_1$	4.071598	304.51	2.2958	3.014741	411.26	1.6654	3.021721	410.31	1.7302
$S_0 \rightarrow S_2$	4.938037	251.08	0.1105	3.511406	353.09	0.0011	3.110259	398.63	0.0024
$S_0 \rightarrow S_3$	5.471744	226.59	0.0000	3.613332	343.13	0.0630	3.660484	338.71	0.1407
$S_0 \rightarrow S_4$	5.669925	218.67	0.0182	4.015294	308.78	0.0104	3.990995	310.66	0.0108
$S_0 \rightarrow S_5$	5.678494	218.34	0.0233	4.018938	308.50	0.0114	3.994466	310.39	0.0120
$S_0 \rightarrow S_6$	5.764564	215.08	0.0038	4.153298	298.52	0.0001	4.118941	301.01	0.0047
$S_0 \rightarrow S_7$	6.519653	190.17	0.2225	4.307551	287.83	0.0850	4.273109	290.15	0.0662
$S_0 \rightarrow S_8$	6.808580	182.10	0.3470	4.693706	264.15	0.3179	4.471123	277.30	0.2699

Table 14 Results on $S_0 \rightarrow S_n$ ($n = 1, 2,\ldots, 8$) absorption spectra of DPHHTO in DMSO

	CI-S			TD-SCF			CS INDO SDT-CI		
	ΔE (eV)	λ (nm)	f	ΔE (eV)	λ (nm)	f	ΔE (eV)	λ (nm)	f
$S_0 \rightarrow S_1$	4.033320	307.40	2.2967	2.980892	415.93	1.7016	2.858624	433.72	1.9034
$S_0 \rightarrow S_2$	4.887042	253.70	0.1131	3.514990	352.73	0.0014	2.932387	422.81	0.0052
$S_0 \rightarrow S_3$	5.477062	226.37	0.0000	3.596352	344.75	0.0668	3.471878	357.11	0.1433
$S_0 \rightarrow S_4$	5.663191	218.93	0.0208	4.009840	309.20	0.0105	3.968385	312.43	0.0110
$S_0 \rightarrow S_5$	5.672519	218.57	0.0271	4.013474	308.92	0.0128	3.973854	312.00	0.0125
$S_0 \rightarrow S_6$	5.733906	216.23	0.0037	4.143858	299.20	0.0000	4.081248	303.79	0.0037
$S_0 \rightarrow S_7$	6.503239	190.65	0.2213	4.278122	289.81	0.0792	4.165577	297.64	0.0577
$S_0 \rightarrow S_8$	6.781395	182.83	0.3677	4.682008	264.81	0.3258	4.395825	282.05	0.2868

same trend of the whole spectrum. For both the solvents, $S_0 \rightarrow S_4$ and $S_0 \rightarrow S_5$ transitions are quasi-degenerate and present closer oscillator strengths values. Very low intensities are observable for $S_0 \rightarrow S_6$ transition, at TD-DFT level. Concerning oscillator strengths, in general, the first transitions increase their intensities, while the last ones decrease, passing from vacuum to solvated phase.

Regarding the excited states geometries, solvent effect is not particularly marked. Light or negligible structural modifications are shown with respect to the results as obtained in vacuum phase. The geometrical element which seems more sensible is the central bond angle. For all the structures, passing from vacuum to methanol to DMSO, a progressive spread is observable, in particular for S_1, S_2, S_7 and S_8.

4 Conclusions

The present theoretical study has led to the following conclusions:

- At room temperature, both in vacuum and in solvent, the di-ketonic isomer (DPHDDO) presence is negligible with respect to the keto-enolic isomer (DPHHTO), as observed for curcumin.
- Full geometry optimizations at DFT B3LYP/6-311g(*p*,*d*) level lead to structure in good agreement with X-ray experimental data.
- From a spectroscopic point of view, TD-DFT and CS INDO SDT-CI results are in reasonable agreement, while CI-S method does not provide reliable ones. The crucial importance of poly-excitation for the correct description of electronic properties is noted. This aspect has relevant consequences in the excited states geometries optimizations.
- Through the comparison of the calculations as obtained through the three utilized methods, concerning the excited states geometries optimizations, the best results are achieved by CAS-SCF technique, which provides diverse structures for the different excited states.
- Owing to the excited states geometries optimizations, the energetic order of the states is partially modified. Intersections between the potential energy hyper-surfaces are supposed.
- The implicit treatment of the solvent effects does not lead to sensitive changes in the geometry, with respect to the vacuum. As for curcumin, a red shift and

modifications of the transitions intensities are notable. An explicit approach may be suggested for additional studies in the future.

The obtained results may be of large applicative interests. Since the curcuminoids are considered as potential ligands for complexes formation with metallic ions of pharmaceutical, medical–physical, therapeutic and technological interest, on the basis of the present study, a photomodulated release of the metallic ion may be guessed. In other words, exciting the system with photons of appropriate frequencies, an important geometry modification should be induced, with consequent release of the metallic centre in the environment.

Acknowledgments The authors are grateful to the "Laboratorio di Calcolo Scientifico Avanzato Interdipartimentale dell'Università degli Studi di Modena e Reggio Emilia" and to the Georgia Institute of Technology for computing facilities.

References

1. Gafner S, Lee SK, Cuendet M, Barthelemy S, Vergnes L, Labidalle S, Mehta RG, Boone CW, Pezzuto JM (2004) Phytochemistry 65:2849
2. Maheshwari RK, Singh AK, Gaddipati J, Srimal RC (2006) Life Sci 78:2081
3. Srichairatanakool S, Thephinlap C, Phisalaphong C, Porter JB, Fucharoen S (2007) Med Chem 3:469
4. John VD, Kuttan G, Krishnankutty K (2002) J Exp Clin Cancer Res 21:219
5. Shen L, Ji HF (2007) Spectrochim Acta A 67:619
6. Jiao Y, Wilkinson JIV, Pietsch EC, Buss JL, Wang W, Planalp R, Torti FM, Torti SV (2006) Free Radic Biol Med 40:1152
7. Borsari M, Ferrari E, Grandi R, Saladini M (2002) Inorg Chim Acta 328:61
8. Bussl JL, Torti FM, Torti SV (2003) Curr Med Chem 10:1021
9. Benassi E, Spagnolo F (2009) J Sol Chem (in press)
10. Benassi R, Ferrari E, Lazzari S, Spagnolo F, Saladini M (2008) J Mol Struct 892:168
11. Miertus S, Scrocco E, Tomasi J (1981) Chem Phys 55:117
12. Miertus S, Tomasi J (1982) Chem Phys 65:239
13. Cossi M, Barone V, Cammi J (1996) Chem Phys 255:327
14. Frisch MJ, Trucks GW, Schlegel HB, Scuseria GE, Robb MA, Cheeseman JR, Montgomery JA Jr, Vreven T, Kudin KN, Burant JC, Millam JM, Iyengar SS, Tomasi J, Barone V, Mennucci B, Cossi M, Scalmani G, Rega N, Petersson GA, Nakatsuji H, Hada M, Ehara M, Toyota K, Fukuda R, Hasegawa J, Ishida M, Nakajima T, Honda Y, Kitao O, Nakai H, Klene M, Li X, Knox JE, Hratchian HP, Cross JB, Adamo C, Jaramillo J, Gomperts R, Stratmann RE, Yazyev O, Austin AJ, Cammi R, Pomelli C, Ochterski JW, Ayala PY, Morokuma K, Voth GA, Salvador P, Dannenberg JJ, Zakrzewski VG, Dapprich S, Daniels AD, Strain MC, Farkas O, Malick DK, Rabuck AD, Raghavachari K, Foresman JB, Ortiz JV, Cui Q, Baboul AG, Clifford S, Cioslowski J, Stefanov BB, Liu G, Liashenko A, Piskorz P, Komaromi I, Martin RL, Fox DJ, Keith T, Al-Laham MA, Peng CY, Nanayakkara A, Challacombe M, Gill PMW, Johnson B, Chen W, Wong MW, Gonzalez C, Pople JA (2003) Gaussian 03. Gaussian Inc., Pittsburgh
15. Foresman B, Head-Gordon M, Pople JA, Frisch MJ (1992) J Phys Chem 96:135
16. Momicchioli F, Baraldi I, Bruni MC (1983) Chem Phys 82:229
17. Miertus S, Kysel O (1977) Chem Phys 21:27
18. Costanciel R, Tapia O (1978) Theor Chem Acta 48:383
19. Miertus S, Kysel O (1979) Chem Phys Lett 65:395
20. Tomasi J, Persico M (1994) Chem Rev 94:3027
21. Mostad A, Pedersen U, Rasmussen PB, Lawesson S-O (1983) Acta Chem Scand B 37:901
22. Ohno K (1964) Theor Chim Acta 2:219
23. Klopman G (1964) J Am Chem Soc 86:4550
24. Mataga N, Nishimoto K (1957) Z Phys Chem 12:335
25. Mataga N, Nishimoto K (1957) Z Phys Chem 13:140